

## Study of three quasi-two-body channels from $\pi^+p$ interactions at 3.9 GeV/c\*

B. Haber,<sup>†</sup> M. F. Hodous, R. I. Hulsizer, V. Kistiakowsky, A. Levy,<sup>‡</sup> I. A. Pless,  
R. A. Singer,<sup>§</sup> J. Wolfson, and R. K. Yamamoto

Laboratory for Nuclear Science, Massachusetts Institute of Technology, Cambridge, Massachusetts 02139

(Received 16 September 1974)

The  $p\pi^+\pi^0$  and  $p\pi^+\pi^+\pi^-$  final states from  $\pi^+p$  interactions at 3.9 GeV/c have been analyzed by the prism-plot technique and the following three quasi-two-body channels have been studied in detail:  $\pi^+p \rightarrow \rho^+p$ ,  $\pi^+p \rightarrow \pi^0\Delta^{++}$ , and  $\pi^+p \rightarrow \rho^0\Delta^{++}$ . Results are presented on cross sections, differential cross sections, and single and joint spin density matrix elements. These are compared with the Dar-Watts-Weisskopf absorption model and Reggeized pion-exchange model predictions. Relations among joint spin density matrix elements for  $\rho^0\Delta^{++}$  are compared with quark-model predictions.

### I. INTRODUCTION

A large percentage of high-energy interactions proceed through quasi-two-body channels, and such reactions are particularly suited for comparison with dynamical models because of the relative simplicity of the two-body case. However, a clean separation of the channel under consideration is essential for such a study. The prism-plot analysis technique<sup>1,2</sup> for bubble-chamber data which uses a complete set of kinematic variables, results in a very clean separation, reducing the background contribution due to other channels to a minimum.

In this paper we report the results for a study of three quasi-two-body reactions produced in a hydrogen bubble chamber by 3.9-GeV/c pions:

$$\pi^+p \rightarrow \rho^+p, \quad (1)$$

$$\pi^+p \rightarrow \pi^0\Delta^{++}, \quad (2)$$

$$\pi^+p \rightarrow \rho^0\Delta^{++}. \quad (3)$$

These have been separated from the other channels present in the final states  $\pi^+p \rightarrow p\pi^+\pi^0$  [for reactions (1) and (2)] and  $\pi^+p \rightarrow p\pi^+\pi^+\pi^-$  [for reaction (3)] by the prism-plot technique. The analysis of the three-body final state has been described in a previous paper,<sup>1</sup> as have some of the results for reaction (1).<sup>3</sup>

We compare our data with the predictions of the absorption model as modified by Dar, Watts, and Weisskopf (DWW)<sup>4</sup> and a Reggeized pion-exchange model<sup>5</sup> for those reactions for which pion exchange is possible. We also compare relations among the joint density matrix elements of reaction (3) with quark-model predictions.<sup>6</sup>

In Sec. II, we discuss the details of this experiment and give the total cross sections. In Secs. III–V we present the results for reactions (1)–(3). Cross sections, production and decay angular distributions, and density matrix elements as well as joint density matrix elements for reaction (3)

are compared with the predictions of the theoretical models. In Sec. VI we discuss our results and present our conclusions.

### II. EXPERIMENTAL DETAILS

The data reported in this paper were obtained from 300 000 pictures of 3.9-GeV/c pions in the ANL 30-in. hydrogen bubble chamber. The experiment yielded 27 149 two-prong and 16 043 four-prong events. 70% of the events were measured by PEPR (precision encoding and pattern recognition) and the other 30% were hand measured. The measurements were analyzed using TVGP and SQUAW. Ionization information was measured by PEPR or estimated visually for the hand-measured events and was used in classifying the events. A hypothesis in a higher-constraint class was preferred to a hypothesis in a lower-constraint class. Events which were ambiguous within the same class of constraints were assigned to the hypothesis with the minimum  $\chi^2$ .

From this analysis we obtained 3095 events of the type  $\pi^+p \rightarrow p\pi^+\pi^0$ , of which 2546 are unique, and 3859 events of the type  $\pi^+p \rightarrow p\pi^+\pi^+\pi^-$ , of which 3746 are unique. The corresponding cross sections are  $\sigma(\pi^+p \rightarrow p\pi^+\pi^0) = 2.30 \pm 0.06$  mb and  $\sigma(\pi^+p \rightarrow p\pi^+\pi^+\pi^-) = 3.48 \pm 0.06$  mb. The uncertainties given here and throughout this paper are statistical unless otherwise noted. We obtained these cross sections by normalizing the  $\pi^+p$  total cross section at 3.9 GeV/c (Ref. 7) to the total number of events after correction for scanning and measuring losses and a loss of small-angle elastic scatters.<sup>8</sup>

In Figs. 1 and 2 we show the invariant-mass distributions before prism-plot analysis. Figure 1 gives the  $\pi^+\pi^0$  and  $p\pi^+$  invariant-mass distributions for the  $p\pi^+\pi^0$  final state, and Fig. 2 gives the  $\pi^+\pi^-$  and  $p\pi^+$  invariant-mass distributions for the  $p\pi^+\pi^+\pi^-$  final state. Clearly defined  $\rho$  and  $\Delta^{++}$  peaks are seen in these distributions. After prism-

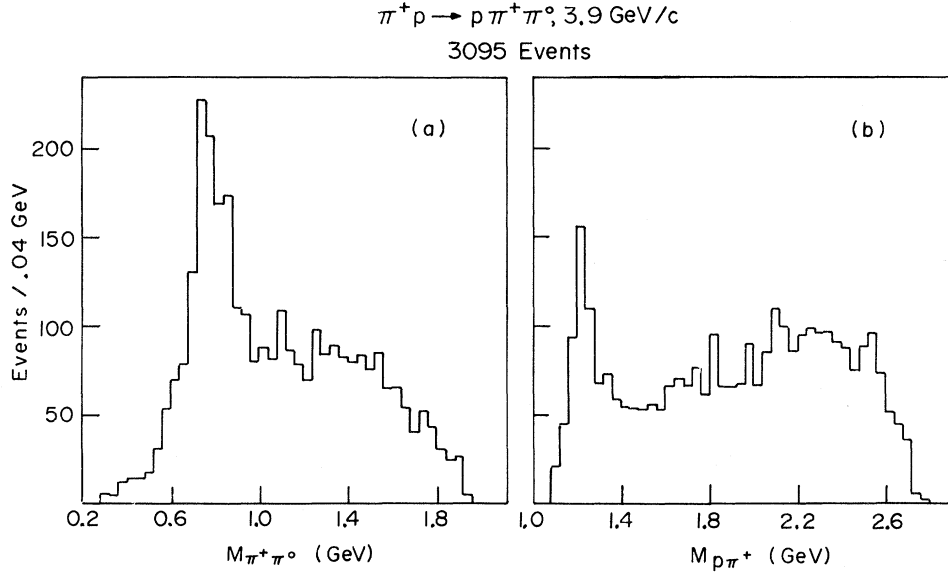


FIG. 1. Invariant-mass distributions for  $\pi^+ p \rightarrow p \pi^+ \pi^0$  at 3.9 GeV/c. (a)  $\pi^+ \pi^0$  invariant mass; (b)  $p \pi^+$  invariant mass.

plot separation we obtain the following cross sections for reactions (1)–(3):  $\sigma(\pi^+ p \rightarrow \rho^+ p) = 0.86 \pm 0.03 \text{ mb}$ ,  $\sigma(\pi^+ p \rightarrow \pi^0 \Delta^{++}) = 0.41 \pm 0.02 \text{ mb}$ , and  $\sigma(\pi^+ p \rightarrow \rho^0 \Delta^{++}) = 1.50 \pm 0.04 \text{ mb}$ . In addition to the statistical uncertainties there is an additional 5% systematic uncertainty estimated for the four-body prism-plot separation of  $\sigma(\pi^+ p \rightarrow \rho^0 \Delta^{++})$ .

### III. THE REACTION $\pi^+ p \rightarrow \rho^+ p$

In Fig. 3 we show the  $\pi^+ \pi^0$  invariant mass for the 957 events selected as  $\rho^+ p$  by prism-plot anal-

ysis. The corresponding cross section,  $0.86 \pm 0.03 \text{ mb}$ , is higher than that derived by ordinary methods in previous experiments.<sup>9,10</sup>

In order to determine the mass and width of the resonance we have performed a  $\chi^2$  fit of a Jackson-modified Breit-Wigner shape<sup>11</sup> to the invariant-mass distribution. The values obtained for the mass and the width of the  $\rho^+$  are  $M = 771 \pm 5 \text{ MeV}$  and  $\Gamma = 160 \pm 18 \text{ MeV}$ . This fit is shown by the continuous curve in Fig. 3. It should be noted that no background contribution was included and the data were fitted by the resonance shape alone.

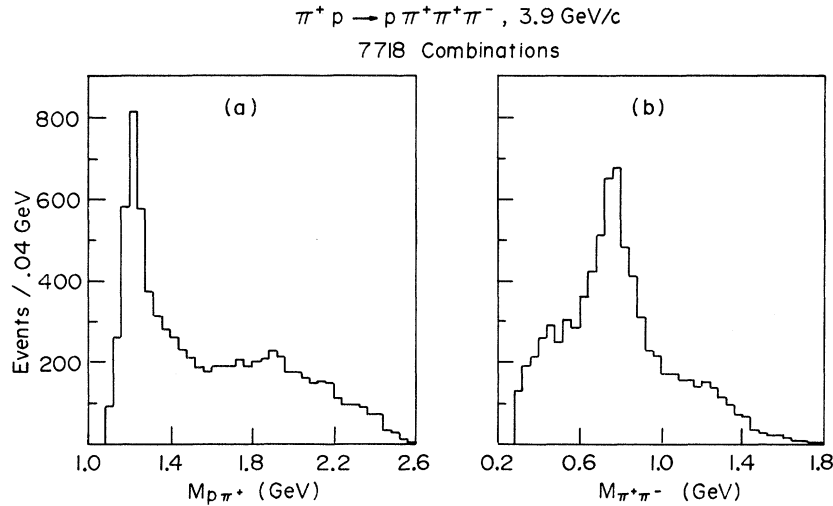


FIG. 2. Invariant-mass distributions for  $\pi^+ p \rightarrow p \pi^+ \pi^+ \pi^-$  at 3.9 GeV/c. (a)  $p \pi^+$  invariant mass; (b)  $\pi^+ \pi^-$  invariant mass. Each event is plotted twice.

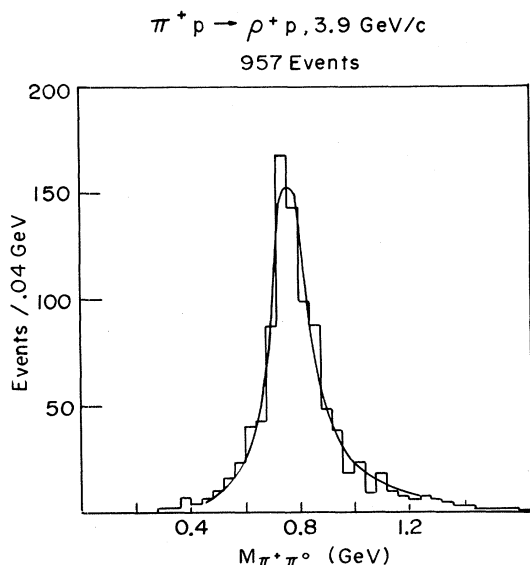


FIG. 3.  $\pi^+\pi^0$  invariant-mass distribution for the events selected as  $\pi^+p \rightarrow \rho^+p$  by the prism-plot analysis. The curve is the result of a fit of a Jackson-modified Breit-Wigner shape to the data with  $M = 771 \pm 5$  MeV and  $\Gamma = 160 \pm 18$  MeV.

The center-of-mass production angular distribution is shown in Fig. 4. The cross section observed for  $\rho^+$  production for  $\theta > 90^\circ$  is  $0.09 \pm 0.01$  mb. In Fig. 5 we present the differential cross section for  $\pi^+p \rightarrow \rho^+p$  as a function of  $t' = |t - t_{\min}|$  for the  $\rho^+$ . The best fit of an exponential ( $e^{-at'}$ ) to the data for  $0.025 < t' < 0.50$  ( $\text{GeV}/c$ )<sup>2</sup> gave  $a = 7.1 \pm 0.5$  ( $\text{GeV}/c$ )<sup>-2</sup>. The agreement with previous data at 4 GeV/c (Refs. 9, 12) is good in the region  $t' < 0.5$  ( $\text{GeV}/c$ )<sup>2</sup>, but our cross sections are significantly larger for  $t' > 0.5$  ( $\text{GeV}/c$ )<sup>2</sup>. The dip observed at  $t' \sim 0.5$  ( $\text{GeV}/c$ )<sup>2</sup> in a high-statistics experiment at 2.67 GeV/c

(Ref. 13) is not apparent in these data. The solid curve gives the result of a calculation of the DWW absorptive model with both  $\pi$  and  $\omega$  exchange. The agreement for  $t' < 0.4$  ( $\text{GeV}/c$ )<sup>2</sup> is good and the inclusion of  $\omega$  exchange does give a shoulder at  $t' > 0.6$  ( $\text{GeV}/c$ )<sup>2</sup> which agrees in shape with the data. Several sets of values for the attenuation coefficients and  $\omega$  coupling constants were tried and it was not possible to bring the model into agreement with the data for  $t' > 0.6$  ( $\text{GeV}/c$ )<sup>2</sup> without causing a broadening of the peak for  $t' < 0.4$  ( $\text{GeV}/c$ )<sup>2</sup> and marked disagreement in this region. The values of the constants used for the DWW curves shown in Figs. 5 and 7 are  $R = 0.85$  F,  $d = 0.1$  F,  $(g^2/4\pi)_{\pi\pi\rho} = 2.6$ ,  $(G^2/4\pi)_{\rho\pi\rho} = 14.7$ ,  $(g^2/4\pi)_{\pi\omega\rho} = 14.0$ ,  $(G_v^2/4\pi)_{\rho\omega\rho} = 5.8$ , and  $(G_t/G_v)_{\rho\omega\rho} = -0.12$ .

The Gottfried-Jackson<sup>14</sup> and Treiman-Yang<sup>15</sup> angular distributions for the  $\rho^+$  decay are shown in Fig. 6. The spin density matrix elements in the Gottfried-Jackson ( $t$  channel) frame have been determined by the method of moments and are shown in Fig. 7 as functions of  $t'$ . Simple non-absorptive pion exchange would predict  $\rho^{00} = 1$  and  $\rho^{1-1} = \text{Re}\rho^{10} = 0$ . The curves give the predictions of the DWW absorptive model with  $\pi$  and  $\omega$  exchange and are not in disagreement with the data within the uncertainties.

To further check the necessity for including  $\omega$  exchange, we have used the tests derived by Ringland and Thews<sup>16</sup> that must be satisfied by the matrix elements of a resonance, if it is produced by the exchange of a single trajectory. In the case of the channel under discussion this test is  $(\text{Re}\rho^{10})^2 - \rho^{11}\rho^{00} = 0$ . The left-hand side of this relation is shown in Table I for different  $t'$  intervals. For  $t' < 0.3$  ( $\text{GeV}/c$ )<sup>2</sup> the relation is violated by more than three standard deviations, which indicates that the reaction  $\pi^+p \rightarrow \rho^+p$  receives con-

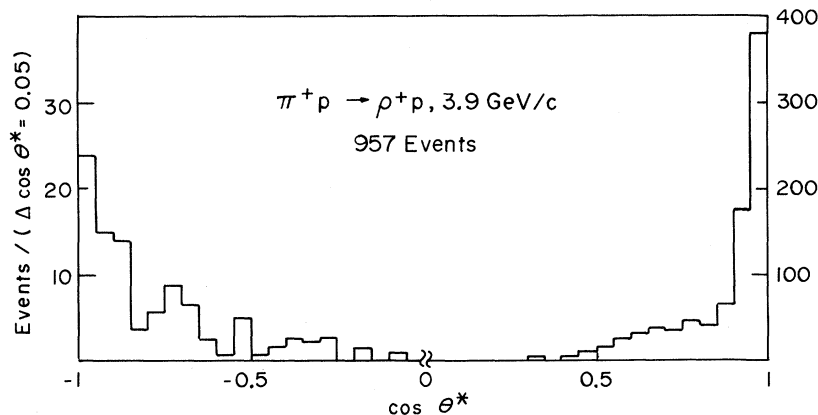


FIG. 4. The center-of-mass production angular distribution of the  $\rho^+$  in the  $\pi^+p \rightarrow \rho^+p$  prism-plot-selected sample.

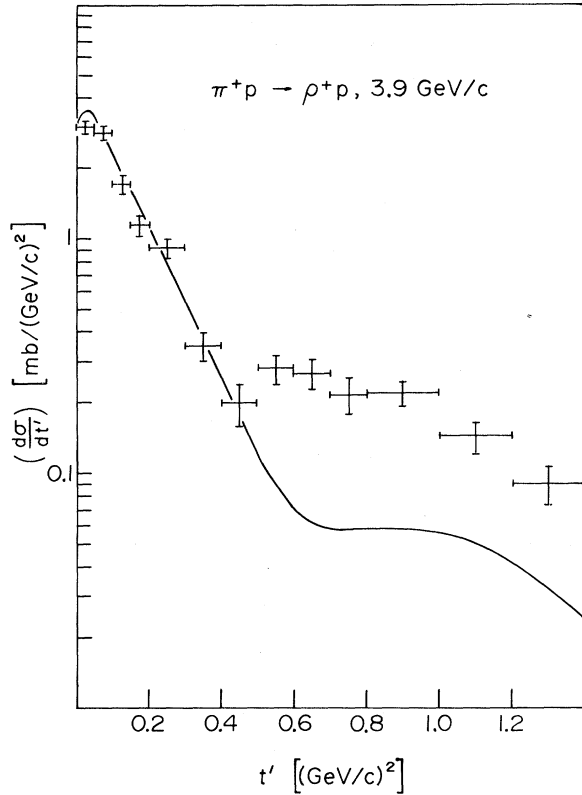


FIG. 5. The differential cross section with respect to  $t'$  for the  $\rho^+$  from events selected as  $\pi^+p \rightarrow \rho^+p$  by prism-plot analysis. The curve gives the prediction of the DWW model with  $\pi$  and  $\omega$  exchange and with  $R = 0.85$  F and  $d = 0.10$  F.

TABLE I. Ringland-Thews test for the  $\rho^+$  from the  $\pi^+p \rightarrow \rho^+p$  prism-plot-selected sample at 3.9 GeV/c.

$t'$ [(GeV/c) <sup>2</sup> ]	$\rho^{00}\rho^{11} - (\rho^{10})^2$
0-0.025	0.12 ± 0.03
0.025-0.05	0.12 ± 0.02
0.05-0.75	0.12 ± 0.02
0.075-0.1	0.12 ± 0.03
0.1-0.2	0.12 ± 0.02
0.2-0.3	0.12 ± 0.02
0.3-0.4	0.12 ± 0.04
0.4-0.5	0.12 ± 0.05
0.5-0.6	0.12 ± 0.04
0.6-0.8	0.07 ± 0.03
0.8-1.0	0.08 ± 0.03
1.0-1.5	0.03 ± 0.03
1.5-2.0	0.07 ± 0.10
2.0-2.5	0.09 ± 0.34
2.5-3.0	0.08 ± 0.39
3.0-3.5	0.02 ± 0.16

tributions from more than one trajectory.

The contributions corresponding to various quantum numbers may be separated by weighting the differential cross section by the appropriate combination of spin density matrix elements. The matrix element  $\rho^{00}$  isolates the unnatural-parity-exchange contribution with no helicity flip in the  $t$  channel.<sup>17</sup> The two combinations  $(\rho^{11} + \rho^{1-1})$  and  $(\rho^{11} - \rho^{1-1})$ , select, respectively, the natural- and unnatural-parity exchange with helicity flip in the  $t$  channel.<sup>18</sup> The results for  $\rho^{00}(d\sigma/dt')$  are shown in Fig. 8 together with the prediction of a Reg-

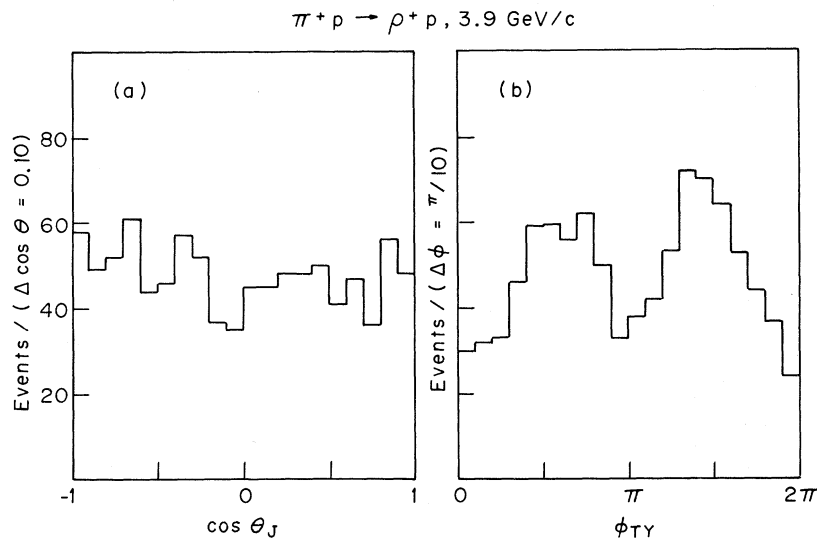


FIG. 6. Angular distributions for the  $\rho^+$  in the  $\pi^+p \rightarrow \rho^+p$  prism-plot-selected sample. (a) The Gottfried-Jackson angular distribution; (b) the Treiman-Yang angular distribution.

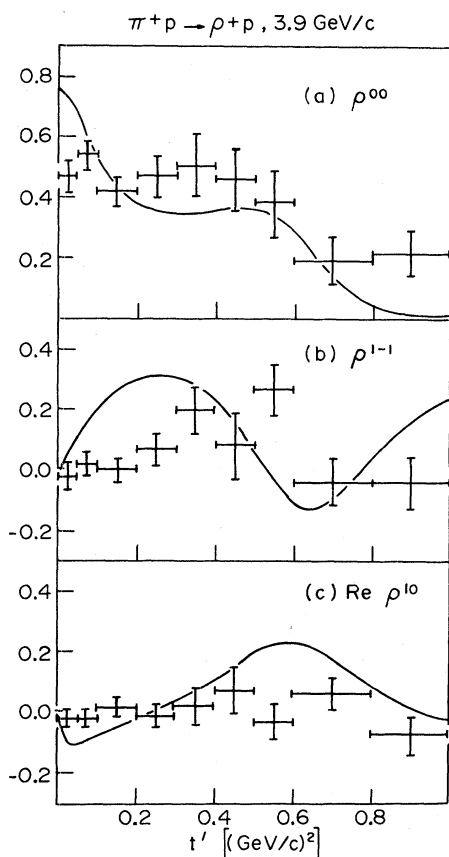


FIG. 7. Density matrix elements as a function of  $t'$  for the  $\rho^+$  in the  $\pi^+ p \rightarrow \rho^+ p$  prism-plot-selected sample. The curves give the predictions of the DWW model with pion exchange and with  $R = 0.85$  F and  $d = 0.10$  F.

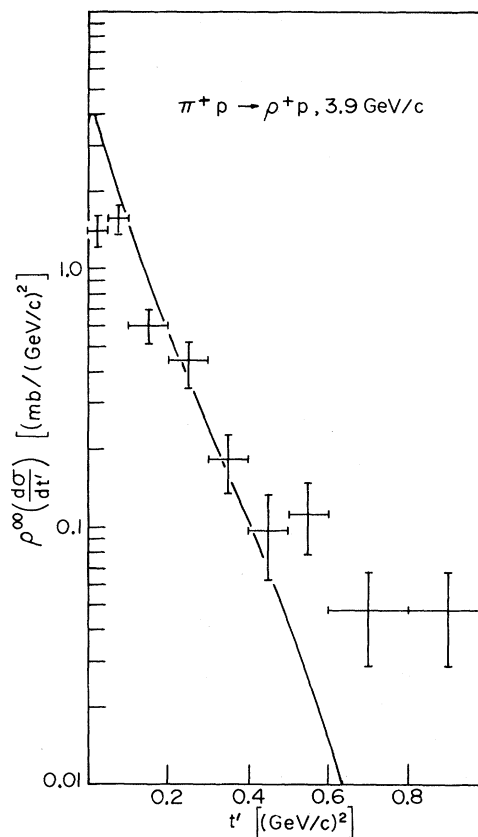


FIG. 8. The weighted differential cross section as a function of  $t'$  for the  $\rho^+$  from the  $\pi^+ p \rightarrow \rho^+ p$  prism-plot-selected sample. The curve gives the prediction of a Reggeized pion-exchange model with  $\alpha' = 1.0$ .

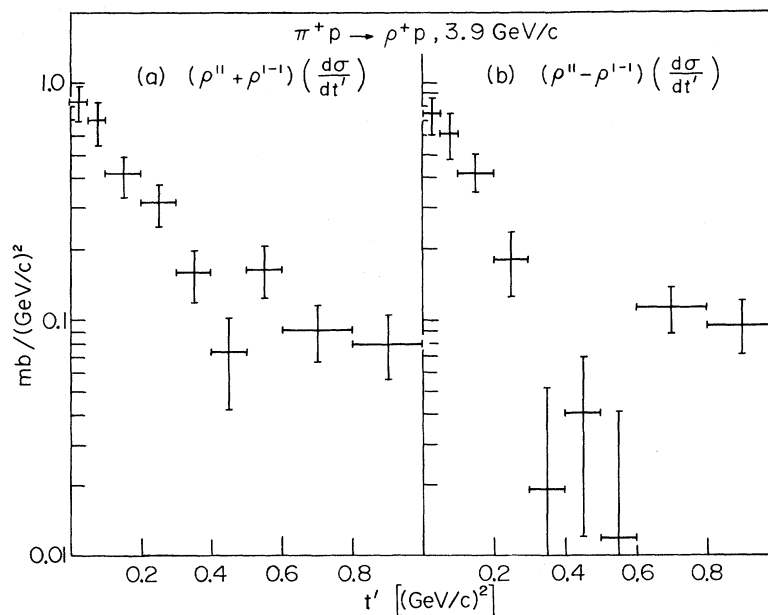


FIG. 9. The weighted differential cross sections as a function of  $t'$  for the  $\rho^+$  from the  $\pi^+ p \rightarrow \rho^+ p$  prism-plot-selected sample. (a) Natural-parity and (b) unnatural-parity exchange contributions.

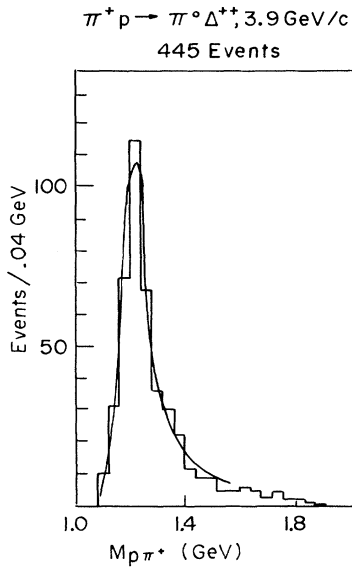


FIG. 10.  $p\pi^+$  invariant-mass distribution for the  $\pi^+p \rightarrow \pi^0\Delta^{++}$  prism-plot-selected sample. The curve is the result of a fit of a Jackson-modified Breit-Wigner shape to the data with  $M = 1220 \pm 5$  MeV and  $\Gamma = 104 \pm 22$  MeV.

geized pion-exchange model.<sup>5</sup> The prediction agrees with the data only in the region  $0.1 < t' < 0.5$   $(\text{GeV}/c)^2$ . The depletion of the weighted cross section in the first bin has been shown not to be due to a loss of events because of scanning bias. The DWW model with  $\omega$  exchange predicts a dip at  $t' \sim 0.5$   $(\text{GeV}/c)^2$  in the natural-parity-exchange contribution,  $(\rho^{11} + \rho^{1-1})(d\sigma/dt')$ , and this is not evident in our data [Fig. 9(a)].

#### IV. THE REACTION $\pi^+p \rightarrow \pi^0\Delta^{++}$

In Fig. 10 we show the  $p\pi^+$  invariant mass for the 445 events selected as  $\pi^0\Delta^{++}$  by prism-plot

analysis. Our cross section for this channel,  $0.41 \pm 0.02$  mb, is in agreement with the values obtained by previous experiments in this energy region.<sup>12,19</sup> The curve gives the best fit of a Jackson-modified Breit-Wigner shape to the  $p\pi^+$  invariant-mass distribution, corresponding to the values  $M = 1220 \pm 5$  MeV and  $\Gamma = 104 \pm 22$  MeV. No background contribution was included in the fitting procedure, evidence again that the prism-plot technique is able to separate the different final states cleanly.

Figure 11 shows the  $\Delta^{++}$  production angular distribution. The cross section for  $\theta > 90^\circ$  (with respect to the direction of the target proton in the center-of-mass system) is  $0.02 \pm 0.01$  mb. Figure 12 shows the differential cross section as a function of  $t'$ . A fit of an exponential ( $e^{-at'}$ ) to the forward peak [ $0.05 < t' < 0.4$   $(\text{GeV}/c)^2$ ] gives  $a = 7.0 \pm 1.0$   $(\text{GeV}/c)^{-2}$ . The dip at  $t' \approx 0.5$   $(\text{GeV}/c)^2$  is expected for  $\rho$  exchange, since the  $\rho$  trajectory has a zero at this value of  $t'$ , and has been reported previously in other experiments.<sup>12,19</sup> Our differential cross sections also agree in magnitude with the previous results at 4 GeV/c.<sup>12,19</sup> The solid curve in Fig. 12 is the prediction of the DWW model assuming  $\rho$  exchange which does not agree with the experimental distribution. The values of the constants used are  $R = 0.85$  F,  $d = 0.1$  F,  $(g^2/4\pi)_{\rho p\pi} = 2.6$ , and  $(G_1^2/4\pi)_{\rho\rho\Delta} = 36$ . The dashed curve gives the  $\pi^-p \rightarrow \pi^0n$  differential cross section from a high-statistics experiment at 3839 MeV/c.<sup>20</sup> Both this and the reaction under consideration in this section are charge-exchange processes which one would expect to be dominated by the exchange of the same particles or trajectories. The agreement between the shapes of the experimental differential cross sections is, in fact, fairly good.

The Gottfried-Jackson and Treiman-Yang angu-

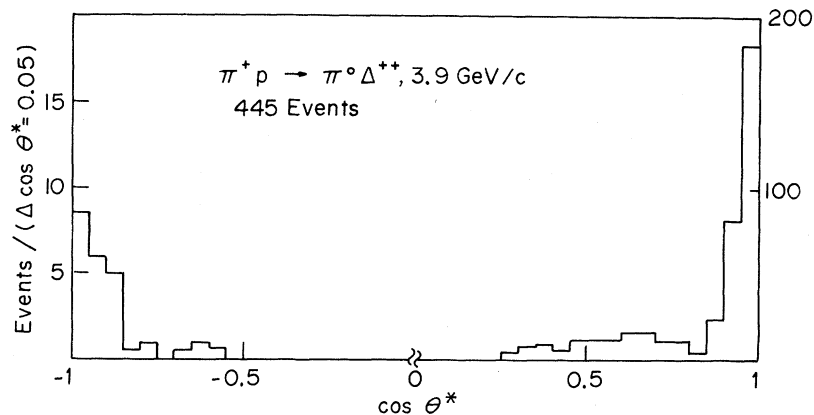


FIG. 11. The center-of-mass production angular distribution of the  $\Delta^{++}$  in the  $\pi^+p \rightarrow \pi^0\Delta^{++}$  prism-plot-selected sample.

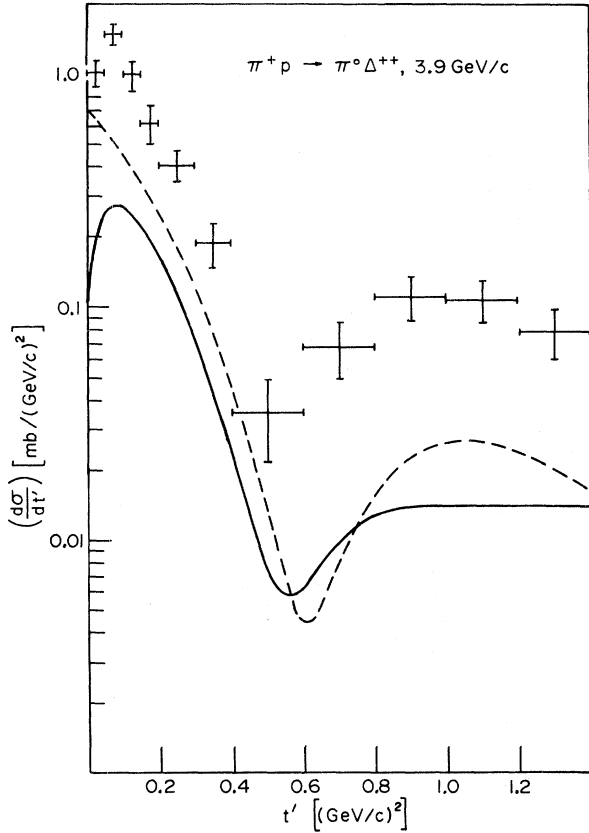


FIG. 12. The differential cross sections as a function of  $t'$  for the  $\Delta^{++}$  in the  $\pi^+p \rightarrow \pi^0\Delta^{++}$  prism-plot-selected sample. The solid curve gives the prediction of the DWW model with  $\rho$  exchange and with  $R = 0.85$  F and  $d = 0.1$  F. The dashed curve shows the  $\pi^-p \rightarrow \pi^0n$  differential cross section at 3.839 GeV/c (see Ref. 20).

TABLE II. Ringland-Thews test for the  $\Delta^{++}$  from the  $\pi^+p \rightarrow \pi^0\Delta^{++}$  prism-plot-selected sample at 3.9 GeV/c.

$t' [(\text{GeV}/c)^2]$	$\rho_{3/2,3/2}\rho_{1/2,1/2} - (\text{Re}\rho_{3/2,1/2})^2 - (\text{Re}\rho_{3/2,-1/2})^2$
0-0.05	$0.05 \pm 0.03$
0.05-0.1	$0.06 \pm 0.02$
0.1-0.2	$0.05 \pm 0.02$
0.2-0.3	$0.03 \pm 0.03$
0.3-0.4	$-0.04 \pm 0.06$
0.4-0.6	$0.02 \pm 0.12$
0.6-0.8	$0.01 \pm 0.07$
0.8-1	$0.05 \pm 0.05$
1-1.5	$0.04 \pm 0.03$
1.5-2	$0.05 \pm 0.05$

lar distributions for the decay of the  $\Delta^{++}$  are shown in Fig. 13. The  $t$ -channel spin density matrix elements as a function of  $t'$  are shown in Fig. 14 together with curves giving the predictions of the  $\rho$ -exchange DWW model. The curves for  $\rho_{3/2,3/2}$  and  $\text{Re}\rho_{3/2,1/2}$  are in reasonable agreement with the data, but that for  $\rho_{3/2,-1/2}$  is not.

In order to check the possibility of contributions of more than one trajectory to the process  $\pi^+p \rightarrow \pi^0\Delta^{++}$ , we applied the Ringland-Thews test for this process,  $\rho_{3/2,3/2}\rho_{1/2,1/2} - (\text{Re}\rho_{3/2,1/2})^2 - (\text{Re}\rho_{3/2,-1/2})^2 = 0$ . The values for the left-hand side of this relation are shown in Table II for different  $t'$  intervals. The expression is consistent with zero for all the intervals given with a confidence level of  $\sim 10\%$ , but there is a three-standard-deviation effect in the region  $0.05 < t' < 0.2 (\text{GeV}/c)^2$ . A significant effect has been observed in other experiments<sup>19</sup> and calculations

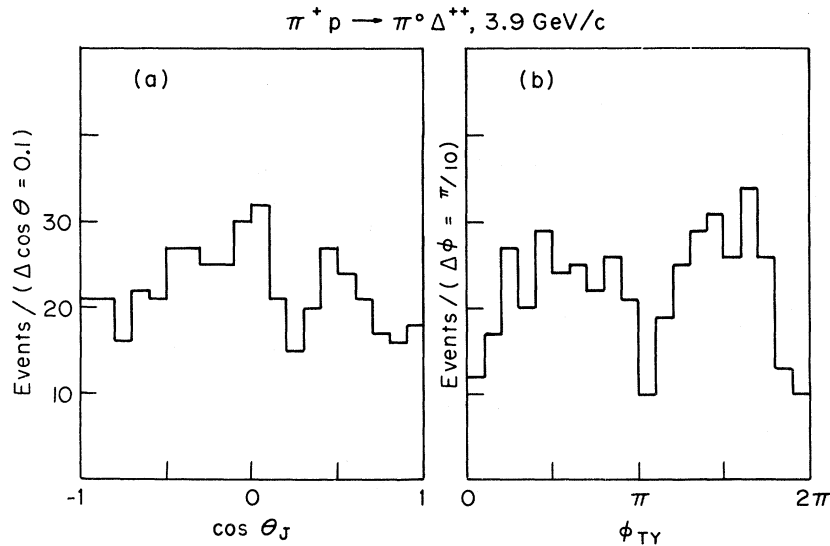


FIG. 13. Angular distributions for the  $\Delta^{++}$  in the  $\pi^+p \rightarrow \pi^0\Delta^{++}$  prism-plot-selected sample. (a) The Gottfried-Jackson angular distribution; (b) the Treiman-Yang angular distribution.

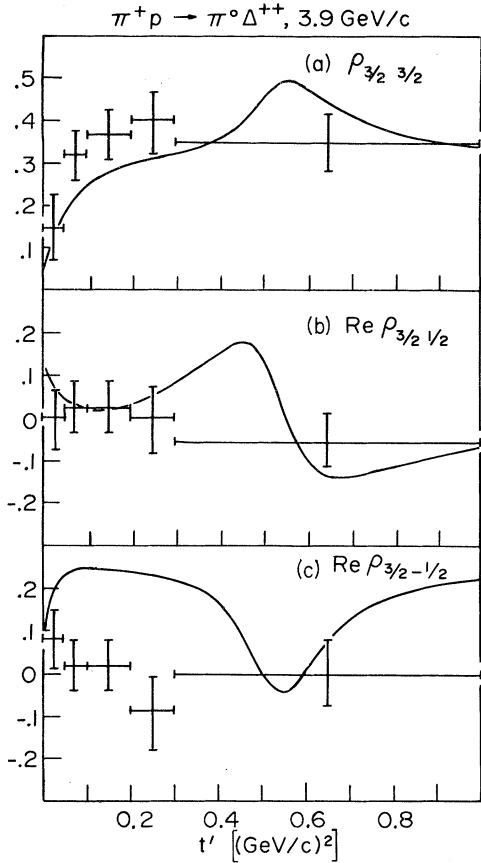


FIG. 14. The density matrix elements as a function of  $t'$  for the  $\Delta^{++}$  from the  $\pi^+p \rightarrow \pi^0\Delta^{++}$  prism-plot-selected sample. The curves are the predictions of the DWW model with  $\rho$  exchange and with  $R=0.85$  F and  $d=0.1$  F.

based on a model including more than one trajectory have been carried out.<sup>21</sup>

## V. THE REACTION $\pi^+p \rightarrow \rho^0\Delta^+$

### A. $\rho^0$ and $\Delta^+$ production and decay

In Fig. 15 we show the  $p\pi^+$  and  $\pi^+\pi^-$  invariant-mass distributions for the 1350 events in the sample selected as  $\pi^+p \rightarrow \rho^0\Delta^+$  by prism-plot analysis. The value found for the cross section of this channel,  $1.50 \pm 0.04$  mb, is higher than results of previous experiments in the energy region 3.5–5.0

GeV/c.<sup>22–25</sup> It should be noted that the determination of the cross section of a double-resonance process, using ordinary methods of analysis, presents serious problems and is generally model-dependent. This may explain both the variation of the previous results over this region and their difference from the present value.

Jackson-modified Breit-Wigner shapes were fitted to the  $(p\pi^+)$  and  $(\pi^+\pi^-)$  invariant-mass distributions and the curves in Fig. 15 show the results. These best fits occurred for the following values of the masses and widths:  $M_{\Delta^{++}} = 1219 \pm 5$  MeV,  $\Gamma_{\Delta^{++}} = 120 \pm 21$  MeV,  $M_{\rho^0} = 775 \pm 6$  MeV, and  $\Gamma_{\rho^0} = 187 \pm 22$  MeV. No background contribution was included in the fitting procedure. The statistical uncertainties do not permit an observation of the sharp shoulder between 950 and 980 MeV previously observed in the  $\pi^+\pi^-$  invariant-mass distribution.<sup>26</sup>

The differential cross section for  $\rho^0\Delta^{++}$  production as a function of  $t'$  is shown in Fig. 16. Exponentials ( $e^{-at'}$ ) were fitted to the data in two regions with the following results:  $a = 15.6 \pm 1.3$  (GeV/c)<sup>-2</sup> for  $t' < 0.08$  (GeV/c)<sup>2</sup> and  $a = 3.6 \pm 0.1$  (GeV/c)<sup>-2</sup> for  $0.3 < t' < 1.5$  (GeV/c)<sup>2</sup>. The curve gives the prediction of the DWW model with pion exchange and with  $R=0.85$  F and  $d=0.1$  F. The agreement with the experimental values is good.

In Fig. 17 we show the decay angular distributions of the  $\Delta^{++}$  and  $\rho^0$ . The Treiman-Yang angular distributions are isotropic, in agreement with the prediction of a spin-zero particle exchange. The Gottfried-Jackson angular distribution of both the  $\Delta^{++}$  and  $\rho^0$  are asymmetric. In Fig. 18 the  $\rho^0$  Gottfried-Jackson angular distribution is plotted for different intervals of  $t'$  and  $M_{\pi^+\pi^-}$  and the asymmetry is seen to be a function of  $t'$  and  $M_{\pi^+\pi^-}$ . In Fig. 19 we plot the  $\rho^0$  decay asymmetry parameter,  $(F-B)/(F+B)$ , as a function of  $M_{\pi^+\pi^-}$  and  $t'$ .  $F$  and  $B$  denote the number of events with a  $\pi^+$  from the decay going forward or backward, respectively, relative to the direction of the incoming  $\pi^+$  in the  $\rho^0$  rest frame. The asymmetry cannot be explained in terms of a freely decaying spin-one particle, and it is generally assumed that an  $s$ -wave  $\pi\pi$  interaction also contributes. The two-dimensional dipion decay angular distribution including both  $s$  and  $p$  waves and their interference<sup>27</sup> is given by

$$W(\theta, \phi) = \frac{3}{4\pi} (\rho^{00} \cos^2\theta + \rho^{11} \sin^2\theta - \sqrt{2} \operatorname{Re} \rho^{10} \sin 2\theta \cos \phi - \rho^{1-1} \sin^2\theta \cos 2\phi) + \frac{\sqrt{3}}{4\pi} (-2\sqrt{2} \operatorname{Re} \rho_{\text{int}}^{10} \sin \theta \cos \phi + 2 \operatorname{Re} \rho_{\text{int}}^{00} \cos \theta) + \frac{1}{4\pi} \rho_s^{00}. \quad (4)$$

In the equation  $\rho_s^{00}$  corresponds to a pure  $s$ -wave contribution and  $\rho_{\text{int}}^{00}$  and  $\rho_{\text{int}}^{10}$  correspond to  $s$ - and  $p$ -wave interference terms. The values of the

spin density matrix elements for the  $\rho^0$  have been determined by the method of moments and are given in Fig. 20. The curves in Figs. 20(a)–20(c)

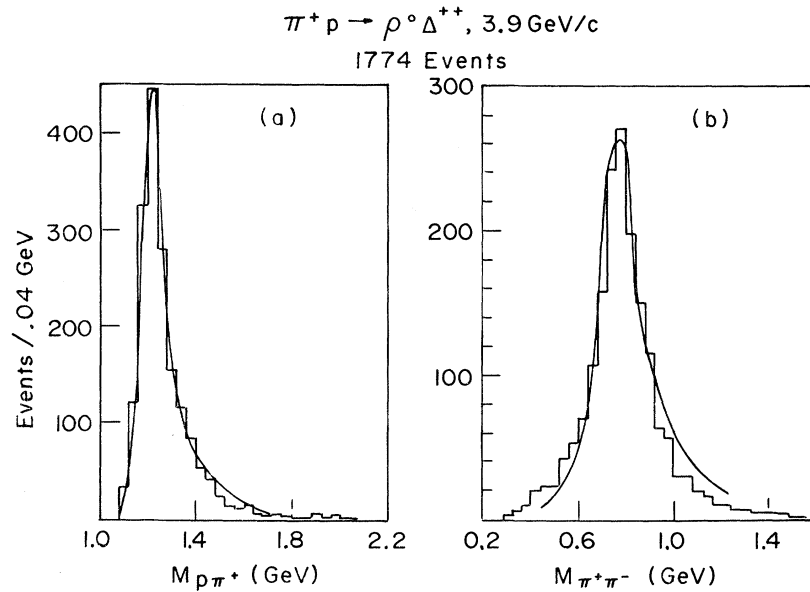


FIG. 15.  $p\pi^+$  and  $\pi^+\pi^-$  invariant-mass distributions for the  $\Delta^{++}$  and the  $\rho^0$  from the  $\pi^+p \rightarrow \rho^0\Delta^{++}$  prism-plot-selected sample. The curves are the results of fits by Jackson-modified Breit-Wigner shapes to the data. (a)  $p\pi^+$  with  $M=1219 \pm 5$  MeV and  $\Gamma=120 \pm 21$  MeV; (b)  $\pi^+\pi^-$  with  $M=775 \pm 6$  MeV and  $\Gamma=187 \pm 22$  MeV.

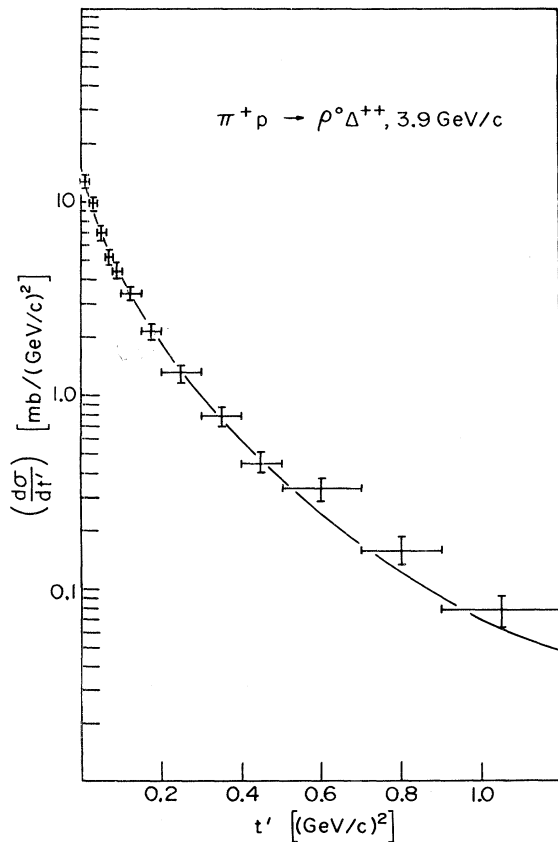


FIG. 16. The differential cross section as a function of  $t'$  for the  $\rho^0$  in the  $\pi^+p \rightarrow \rho^0\Delta^{++}$  prism-plot-selected sample. The curve gives the prediction of the DWW model with  $\pi$  exchange and with  $R=0.85$  F and  $d=0.10$  F.

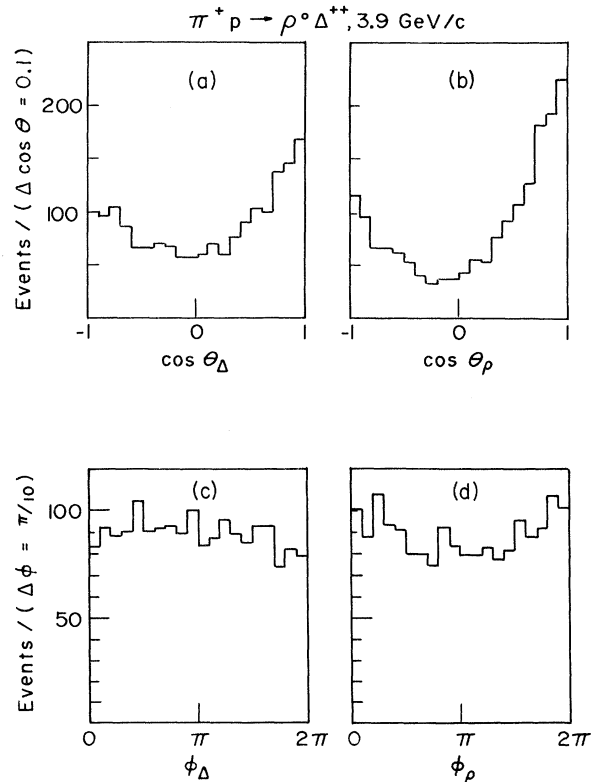


FIG. 17. Angular distributions for the  $\pi^+p \rightarrow \rho^0\Delta^{++}$  prism-plot-selected sample. The Gottfried-Jackson angular distributions of (a) the  $\Delta^{++}$  and (b) the  $\rho^0$ ; the Treiman-Yang angular distributions of (c) the  $\Delta^{++}$  and (d) the  $\rho^0$ .

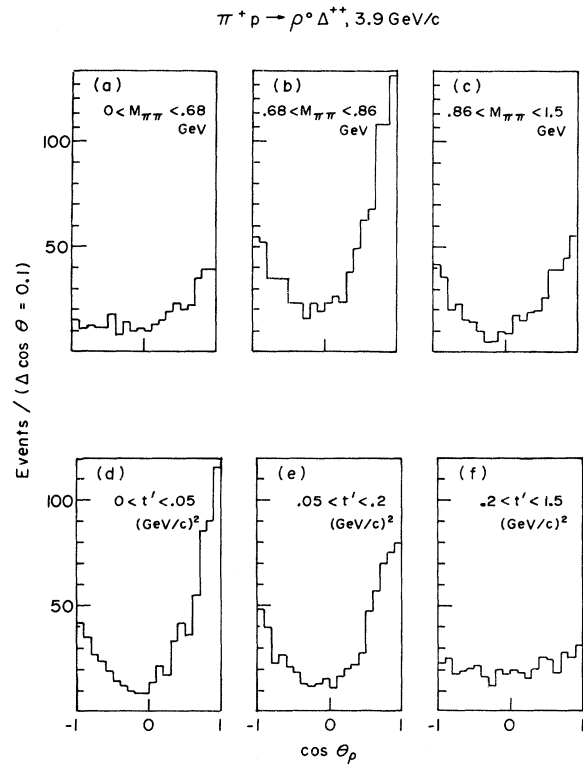


FIG. 18. Gottfried-Jackson decay distribution of the  $\rho^0$  in the  $\pi^+ p \rightarrow \rho^0 \Delta^{++}$  prism-plot-selected sample for different intervals of  $\pi^+\pi^-$  invariant mass and  $t'$ .

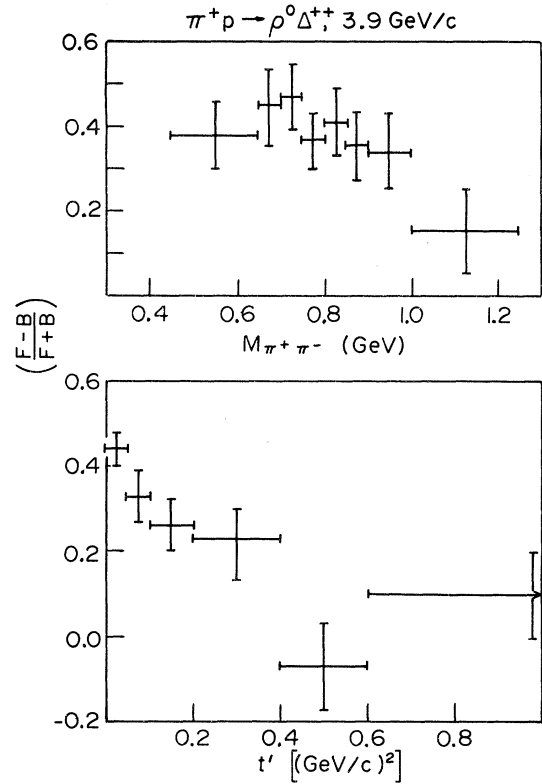


FIG. 19. The asymmetry parameter  $(F-B)/(F+B)$  for the  $\rho^0$  from the  $\pi^+ p \rightarrow \rho^0 \Delta^{++}$  prism-plot-selected sample as a function of (a)  $\pi^+\pi^-$  invariant mass and (b)  $t'$ .

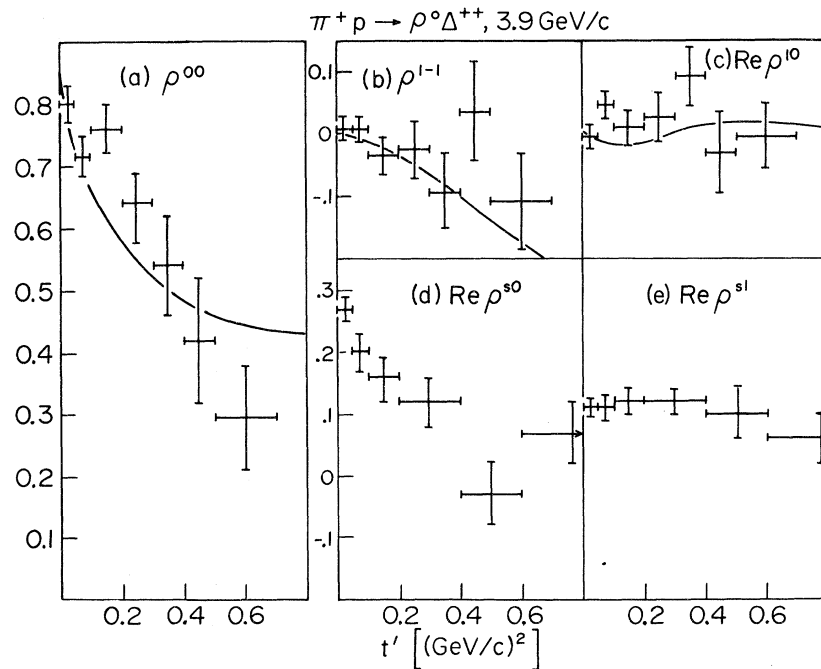


FIG. 20. Density matrix elements for the  $\rho^0$  from the  $\pi^+ p \rightarrow \rho^0 \Delta^{++}$  prism-plot-selected sample as a function of  $t'$ . The curves are the predictions of the DW model with  $\pi$  exchange and with  $R=0.85$  F and  $d=0.1$  F.

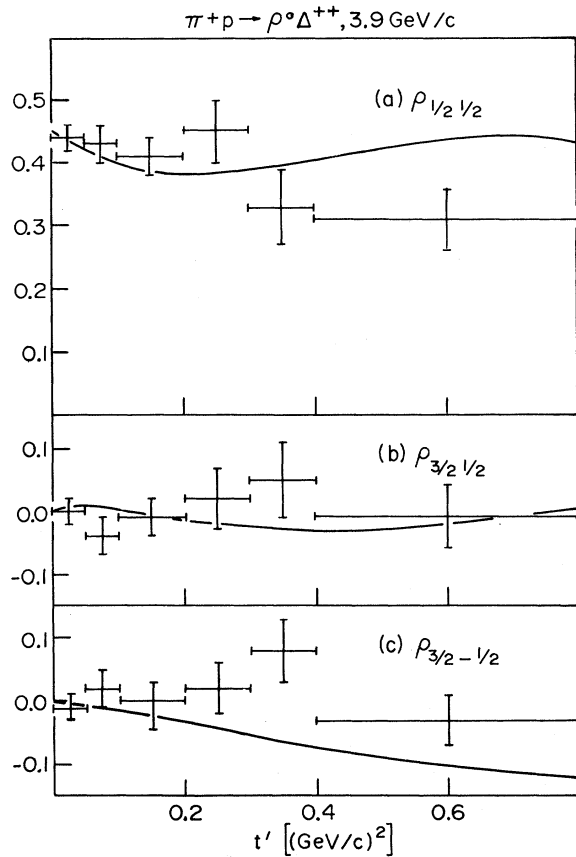


FIG. 21. Density matrix elements for the  $\Delta^{++}$  from the  $\pi^+p \rightarrow \rho^0\Delta^{++}$  prism-plot-selected sample as a function of  $t'$ . The curves are the predictions of the DWW model with  $\pi$  exchange and with  $R=0.85$  F and  $d=0.1$  F.

show the prediction of the DWW model with pion exchange and with  $R=0.85$  F and  $d=0.10$  F. Figures 20(d) and 20(e) show the  $s$ - and  $p$ -wave interference density matrix elements. The first term is a decreasing function of  $t'$  and is related to the observed forward-backward asymmetry. The second term,  $\text{Re}\rho_{int}^{10}$ , is compatible with zero in the whole region. It should be noted that Eq. (4), from which we calculate the interference terms, is related to the  $4 \times 4$  spin density matrix which describes the combined  $s$ - and  $p$ -wave spin state.<sup>28</sup>

In Fig. 21 we give the spin density matrix elements for the  $\Delta^{++}$ . The ordinary spin density matrix elements for both the  $\rho^0$  and  $\Delta^{++}$  are assumed not to be affected seriously by the presence of an  $s$ -wave contribution, which is true when the  $s$ -wave cross section is small compared to that for the  $p$  wave. The curves again show the results of a pion-exchange DWW calculation and agree with the data within statistics.

In order to isolate the contribution of the unnatural-spin-parity exchange to the helicity-zero

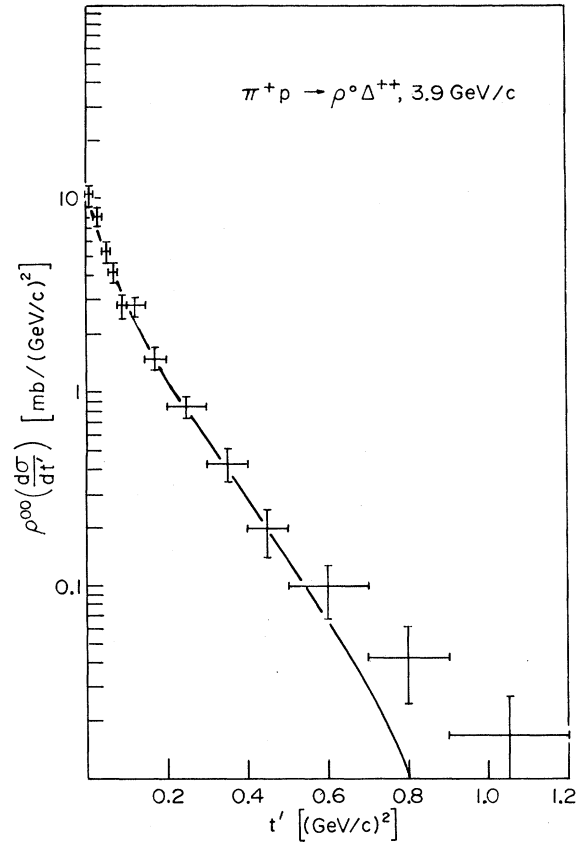


FIG. 22. The weighted differential cross section as a function of  $t'$  for the  $\rho^0$  from the  $\pi^+p \rightarrow \rho^0\Delta^{++}$  prism-plot-selected sample. The curve is the result of a fit by a Reggeized pion-exchange model with  $\alpha' = 0.85$  (GeV/c)<sup>-2</sup>.

state ( $\pi$  exchange) we plot in Fig. 22 the weighted distribution  $\rho^{00}(d\sigma/dt')$ . The curve shown is the best fit to the data of a Reggeized pion-exchange model calculation.<sup>24</sup> This model uses the Born OPE (one-pion-exchange) cross section, with the pion propagator replaced by the expression

$$\frac{1}{t-m_\pi^2} \rightarrow \pi\alpha'(0) \frac{i+e^{-i\pi\alpha}}{2\sin\pi\alpha'} \times \frac{(1+2\alpha)(1+\frac{2}{3}\alpha)\Gamma(\alpha+\frac{1}{2})}{\Gamma(\frac{1}{2})\Gamma(\alpha+1)} \left(\frac{s-u}{2s_0}\right)^\alpha, \quad (5)$$

where  $\alpha = \alpha'(0)(t-m_\pi^2)$  is the pion trajectory. The best fit to the data has a confidence level of 3% ( $\chi^2/\text{ND} = 27/16$ ) and gives  $\alpha' = 0.85 \pm 0.03$  (GeV/c)<sup>-2</sup> and  $2s_0 = 1$ , which are in good agreement with the accepted parameters of the pion trajectory.

#### B. Joint decay angular distributions

In Fig. 23 we present the  $\rho^0$  decay angular distribution for different regions of the  $\Delta^{++}$  decay

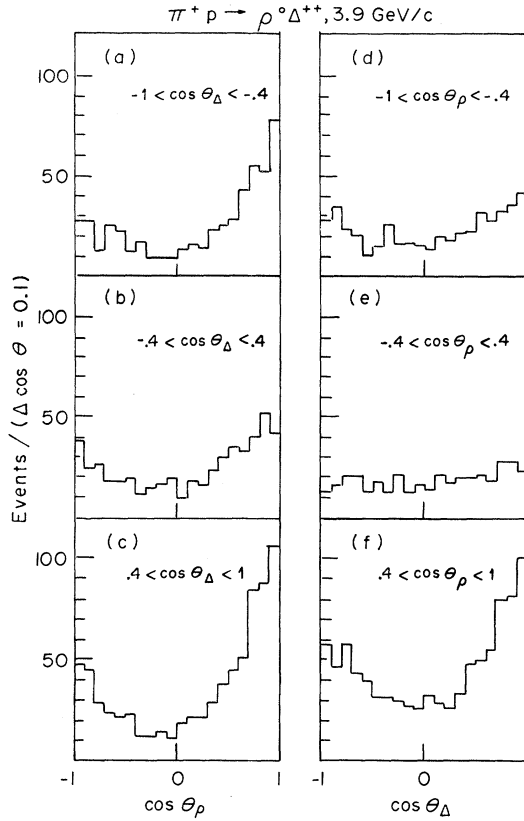


FIG. 23. (a)–(c) Gottfried-Jackson angular distributions for the  $\rho^0$  from the  $\pi^+p \rightarrow \rho^0\Delta^{++}$  prism-plot-selected sample for different intervals of the  $\Delta^{++}$  decay angular distribution. (d)–(f) Gottfried-Jackson angular distributions for the  $\Delta^{++}$  for different intervals of the  $\rho^0$  decay angular distribution.

angular distribution and vice versa. It appears that the two decays are correlated. Similar correlations have been observed in other experiments.<sup>29,30</sup> If there were no correlations between the two decays, then the joint decay distribution  $W(\theta_\rho, \phi_\rho, \theta_\Delta, \phi_\Delta)$  would factor into a product of individual distributions. The correlated distribution may be expressed in terms of a difference,<sup>31</sup>

$$W_c(\theta_\rho, \phi_\rho, \theta_\Delta, \phi_\Delta) = W(\theta_\rho, \phi_\rho, \theta_\Delta, \phi_\Delta) - W_\rho(\theta_\rho, \phi_\rho) - W_\Delta(\theta_\Delta, \phi_\Delta), \quad (6)$$

which may be written in terms of 13 correlation terms defined in Appendix B of Ref. 31. The experimental values are given in Table III. These terms may be expressed as functions of the single decay density matrix elements  $\rho_{mn}$  and  $\rho^{mn}$  (for the  $\Delta^{++}$  and  $\rho^0$ , respectively) and the joint density matrix elements  $\rho_{nn'}$  and  $\rho^{mm'}$ , where

$$\begin{aligned} \rho_{nn'} &= \rho_{nn'}^{11} + \rho_{nn'}^{-1-1} - 2\rho_{nn'}^{00}, \\ \rho^{mm'} &= \rho_{3/2, 3/2}^{mm'} + \rho_{-3/2, -3/2}^{mm'} + \rho_{1/2, 1/2}^{mm'} + \rho_{-1/2, -1/2}^{mm'}. \end{aligned} \quad (7)$$

These relations are also given in Table III. The joint density matrix elements are related to the DWW amplitudes,  $\langle mn|T|\lambda_p\rangle$ , as follows:

$$\rho_{nn'}^{mm'} = \frac{1}{c} \sum_{\lambda_p} \langle mn|T|\lambda_p\rangle \langle m'n'|T|\lambda_p\rangle^*, \quad (8)$$

where  $m$ ,  $n$ , and  $\lambda_p$  are the helicity states of the  $\rho$ ,  $\Delta^{++}$ , and the proton, respectively, and  $c$  is a normalization factor. The 13 correlation terms as calculated from the DWW amplitudes are given in column 3 of Table III. All except terms numbers 6 and 12 are in agreement with the experimental values.

### C. Quark-model predictions

Bialas and Zalevski<sup>32</sup> have derived a number of relations for quark models satisfying various conditions. These involve linear combinations of the density matrix elements which may be expressed as statistical tensors,<sup>33</sup>  $T_{mn}^{kl}$ . These tensors may be defined in terms of moments of the spherical harmonics,  $Y_L^M(\theta, \phi)$  as follows:

$$\begin{aligned} T_{mn}^{22} &= 5\pi\left(\frac{2}{3}\right)^{1/2} \langle Y_m^2(\theta_1, \phi_1) Y_n^2(\theta_2, \phi_2) \rangle, \\ T_{m0}^{20} &= -5\pi\left(\frac{1}{6}\right)^{1/2} \langle Y_m^2(\theta_1, \phi_1) \rangle, \\ T_{0n}^{02} &= 5\pi\left(\frac{1}{3}\right)^{1/2} \langle Y_n^2(\theta_2, \phi_2) \rangle, \end{aligned} \quad (9)$$

where indices 1 and 2 refer to the  $\rho^0$  and  $\Delta^{++}$ , respectively. Using the additivity assumption, according to which only one quark from each hadron takes part in the interaction, they write the  $T_{mn}^{kl}$  in terms of eight quark-quark scattering amplitudes. By the elimination of these amplitudes one gets the class A relations, which are given in Table IV together with experimental values both calculated in the helicity transversity frame and in the Jackson transversity frame. In transversity frames the  $z$  axis is in the direction of the normal to the production plane. They are defined in Appendix A of Ref. 31.

Class B relations are obtained by assuming that the quark-quark spin-flip amplitude satisfies the conditions

$$\langle -\frac{1}{2} + \frac{1}{2} | +\frac{1}{2} - \frac{1}{2} \rangle = \langle +\frac{1}{2} - \frac{1}{2} | -\frac{1}{2} + \frac{1}{2} \rangle, \quad (10)$$

and class C relations are based on the additional assumption

$$\langle +\frac{1}{2} + \frac{1}{2} | -\frac{1}{2} - \frac{1}{2} \rangle = \langle -\frac{1}{2} - \frac{1}{2} | +\frac{1}{2} + \frac{1}{2} \rangle. \quad (11)$$

Class A relations are covariant with respect to arbitrary rotations in the production plane. Class B relations are covariant only with respect to identical rotations for both resonances. Class C relations are not invariant under any rotation.

The observed values for the different relations given in Table IV are evaluated for events with

TABLE III. Correlation terms for  $\pi^+ p \rightarrow \rho^0 \Delta^{++}$ .  $\rho_{mn}$  and  $\rho^{mn}$  are the single spin density matrix elements for the  $\Delta^{++}$  and the  $\rho^0$ , respectively.  $\rho_{nn}^{mn}$  are the joint spin density matrix elements.  $\rho_{n\bar{n}}$  and  $\rho^{n\bar{n}}$  are defined by Eq. (7).<sup>a</sup> The experimental values are calculated for the prism-plot-selected sample at 3.9 GeV/c for  $t' < 0.25 (\text{GeV}/c)^2$  and are compared with predictions of the DWW model with pion exchange.

Correlation term	Experimental	DWW
1. $(\rho_{33}^{\bar{0}} - \rho_{11}^{\bar{0}}) - 2(\rho^{11} - \rho^{00})(\rho_{33} - \rho_{11})$	$0.30 \pm 0.10$	0.37
2. $\text{Re}(\rho^{10}) - 2(\rho_{33} - \rho_{11})\text{Re}(\rho^{10})$	$0.00 \pm 0.03$	-0.02
3. $\rho_{33}^{1,-1} - 2(\rho_{33} - \rho_{11})\rho^{1,-1}$	$-0.03 \pm 0.03$	0.00
4. $\text{Re}(\rho_{31}^{\bar{1}}) - 2(\rho^{11} - \rho^{00})\text{Re}(\rho_{31})$	$0.01 \pm 0.05$	-0.06
5. $\text{Re}(\rho_{3,-1}^{\bar{0}}) - 2(\rho^{11} - \rho^{00})\text{Re}(\rho_{3,-1})$	$0.02 \pm 0.04$	-0.01
6. $\text{Re}(\rho_{31}^{10} - \rho_{31}^{0,-1}) - 2\text{Re}(\rho^{10})\text{Re}(\rho_{31})$	$-0.01 \pm 0.02$	-0.17
7. $\text{Re}(\rho_{31}^{01} - \rho_{31}^{10}) - 2\text{Re}(\rho^{10})\text{Re}(\rho_{31})$	$0.00 \pm 0.02$	0.00
8. $\text{Re}(\rho_{31}^{1,-1}) - \rho^{1,-1}\text{Re}(\rho_{31})$	$0.00 \pm 0.01$	-0.01
9. $\text{Re}(\rho_{31}^{-11}) - \rho^{1,-1}\text{Re}(\rho_{31})$	$-0.01 \pm 0.01$	0.00
10. $\text{Re}(\rho_{3,-1}^{10} - \rho_{3,-1}^{0,-1}) - 2\text{Re}(\rho^{10})\text{Re}(\rho_{3,-1})$	$0.00 \pm 0.02$	0.04
11. $\text{Re}(\rho_{3,-1}^{01} - \rho_{3,-1}^{10}) - 2\text{Re}(\rho^{10})\text{Re}(\rho_{3,-1})$	$-0.01 \pm 0.02$	0.00
12. $\text{Re}(\rho_{3,-1}^{1,-1}) - \rho^{1,-1}\text{Re}(\rho_{3,-1})$	$0.00 \pm 0.01$	0.07
13. $\text{Re}(\rho_{3,-1}^{-11}) - \rho^{1,-1}\text{Re}(\rho_{3,-1})$	$-0.01 \pm 0.01$	0.00

<sup>a</sup>In this table the subscripts represent  $2n, 2n'$ , where  $n, n'$  are half integral.

TABLE IV. Białas and Zalewski relations for the  $\pi^+ p \rightarrow \rho^0 \Delta^{++}$  prism-plot-selected sample at 3.9 GeV/c.

Relation	Experimental: Jackson transversity frame	Experimental: helicity transversity frame
A1 $T_{00}^{20} = \sqrt{2}T_{00}^{02}$	$0.14 \pm 0.01 = 0.12 \pm 0.02$	$0.14 \pm 0.01 = 0.12 \pm 0.02$
A2 $\text{Re}T_{20}^{22} = \frac{1}{2}\text{Re}T_{20}^{20}$	$-0.04 \pm 0.02 = 0.00 \pm 0.01$	$0.02 \pm 0.02 = -0.01 \pm 0.01$
A3 $\text{Im}T_{20}^{22} = \frac{1}{2}\text{Im}T_{20}^{20}$	$0.01 \pm 0.02 = 0.00 \pm 0.01$	$0.00 \pm 0.02 = 0.00 \pm 0.01$
A4 $\text{Re}T_{02}^{22} = \frac{1}{\sqrt{2}}\text{Re}T_{02}^{02}$	$-0.01 \pm 0.02 = -0.02 \pm 0.01$	$0.01 \pm 0.02 = 0.01 \pm 0.01$
A5 $\text{Im}T_{02}^{22} = \frac{1}{\sqrt{2}}\text{Im}T_{02}^{02}$	$0.01 \pm 0.02 = -0.01 \pm 0.01$	$-0.03 \pm 0.02 = 0.00 \pm 0.01$
A6 $T_{00}^{22} = \frac{1}{2\sqrt{6}} - \frac{1}{\sqrt{2}}T_{00}^{02}$	$0.07 \pm 0.02 = 0.14 \pm 0.01$	$0.07 \pm 0.02 = 0.14 \pm 0.01$
B1 $\text{Re}T_{20}^{20} = \sqrt{2}\text{Re}T_{02}^{02}$	$-0.01 \pm 0.01 = -0.03 \pm 0.02$	$-0.01 \pm 0.01 = 0.03 \pm 0.02$
B2 $\text{Im}T_{20}^{20} = \sqrt{2}\text{Im}T_{02}^{02}$	$0.00 \pm 0.01 = -0.01 \pm 0.02$	$0.00 \pm 0.01 = 0.00 \pm 0.02$
B3 $\text{Re}T_{20}^{22} = \text{Re}T_{02}^{22}$	$-0.04 \pm 0.02 = -0.01 \pm 0.02$	$0.02 \pm 0.02 = 0.01 \pm 0.02$
B4 $\text{Im}T_{20}^{22} = \text{Im}T_{02}^{22}$	$0.01 \pm 0.02 = 0.01 \pm 0.02$	$0.00 \pm 0.02 = -0.03 \pm 0.02$
B5 $\text{Im}T_{2,-2}^{22} = 0$	$-0.02 \pm 0.04 = 0$	$-0.04 \pm 0.04 = 0$
B6 $\text{Im}T_{1,-1}^{22} = 0$	$-0.01 \pm 0.02 = 0$	$0.00 \pm 0.02 = 0$
C1 $\text{Im}T_{20}^{20} = 0$	$0.00 \pm 0.01 = 0$	$0.00 \pm 0.01 = 0$
C2 $\text{Im}T_{02}^{02} = 0$	$-0.01 \pm 0.01 = 0$	$0.00 \pm 0.01 = 0$
C3 $\text{Im}T_{02}^{22} = 0$	$0.01 \pm 0.02 = 0$	$-0.03 \pm 0.02 = 0$
C4 $\text{Im}T_{20}^{22} = 0$	$0.01 \pm 0.02 = 0$	$0.00 \pm 0.02 = 0$
C5 $\text{Im}T_{22}^{22} = 0$	$0.01 \pm 0.04 = 0$	$-0.11 \pm 0.04 = 0$
C6 $\text{Im}T_{11}^{22} = 0$	$-0.02 \pm 0.02 = 0$	$0.01 \pm 0.02 = 0$
C7 $\text{Re}(T_{22}^{22} + T_{2,-2}^{22} + T_{00}^{22}) - \frac{1}{\sqrt{6}} = 0$	$0.35 \pm 0.04 = 0$	$0.31 \pm 0.04 = 0$

$t' < 0.25$  (GeV/c)<sup>2</sup>. The agreement is quite good for class A and class B relations in both reference frames. Class C relation C7 does not hold in either of these reference frames and relation C5 does not hold in the helicity transversity frame. Similar results were obtained in other experiments.<sup>34</sup>

## VI. CONCLUSIONS

The prism-plot analysis of the  $\pi^+p \rightarrow p\pi^+\pi^0$  and  $\pi^+p \rightarrow p\pi^+\pi^+\pi^-$  final states was used to separate three quasi-two-body channels. This separation was clean and isolated the events in the three channels without invariant-mass or momentum transfer cuts, permitting unambiguous comparison of differential cross sections and density matrix elements with the predictions of various models.

The first channel considered was  $\pi^+p \rightarrow \rho^+p$ , the data for which are in partial agreement with the predictions of the DWW absorptive model with pion and  $\omega$  exchange, particularly in the  $t'$  region where  $\pi$  exchange dominates. However, the dip expected in the natural-parity-exchange contribution,  $(\rho^{11} + \rho^{1-1})(d\sigma/dt')$ , at  $t' \sim 0.5$  (GeV/c)<sup>2</sup> due to  $\omega$  exchange is not evident in the data. Application of the Ringland-Thews relations to the data support the conclusion that this channel involves contributions from more than one trajectory.

For the  $\pi^+p \rightarrow \pi^0\Delta^{++}$  channel where pion exchange is not allowed, the predictions of the DWW model with  $\rho$  exchange are in poor agreement with the experimental data. Application of the Ringland-Thews relations indicate that more than one trajectory may contribute to this channel. However, a comparison of these data with those for the reac-

tion  $\pi^-p \rightarrow \pi^0n$  shows that the shapes of the differential cross sections as a function of  $t'$  are very similar. This is to be expected since the same particles or trajectories are expected to be exchanged in these two reactions.

The channel  $\pi^+p \rightarrow \rho^0\Delta^{++}$  is dominated by pion exchange. The data are well described by a pion-exchange DWW model with a radius of 0.85 F, slightly higher than the value of 0.78 F predicted by DWW for our energy. Our data for these channels are also fit by a Reggeized pion-exchange model with a pion trajectory slope  $\alpha' \sim 1$  which is in agreement with values determined in other experiments. The asymmetry of the  $\rho^0$  Gottfried-Jackson decay distribution is explained by an  $s$ - $p$  wave interference. Three of the thirteen correlation terms predicted by the DWW model are not in agreement with the experimental results. A comparison of our data with the quark-model predictions of Biaľas and Zalevski show that all class A and class B relations are satisfied in both the Jackson and the helicity transversity frames, whereas not all of the class C relations are satisfied in either frame.

In conclusion, the predictions of the DWW absorptive model agree with our experimental results for channels and in  $t'$  regions where  $\pi$  exchange is dominant, but are not in good agreement where other exchanges dominate.

## ACKNOWLEDGMENTS

We thank the staff of the ANL 30-in. bubble chamber for their efforts in producing the pictures used in this experiment and the staff of our scanning room for the measurements of the events.

\*This work is supported in part through funds provided by the U. S. Atomic Energy Commission under Contract No. AT(11-1) 3069.

†Present address: The Weizmann Institute of Science, Rehovoth, Israel.

‡On leave of absence from Tel Aviv University, Israel.

§Present address: Argonne National Laboratory, Argonne, Illinois.

<sup>1</sup>J. E. Brau *et al.*, Phys. Rev. Lett. **27**, 1481 (1971).

<sup>2</sup>MIT Data Analysis PEPR (precision encoding and pattern recognition) Programming Note, Physics No. 101, 1971 (unpublished).

<sup>3</sup>B. Haber *et al.*, Phys. Rev. D **10**, 1387 (1974).

<sup>4</sup>A. Dar, T. L. Watts, and V. F. Weisskopf, Nucl. Phys. **B13**, 477 (1969).

<sup>5</sup>B. Haber *et al.*, Phys. Rev. **168**, 1773 (1968).

<sup>6</sup>A. Biaľas and K. Zalevski, Nucl. Phys. **B6**, 465 (1968).

<sup>7</sup>A. Citron *et al.*, Phys. Rev. **144**, 1101 (1966).

<sup>8</sup>P. L. Bastien *et al.*, Phys. Rev. D **3**, 2047 (1971).

<sup>9</sup>Aachen-Berlin-Birmingham-Bonn-Hamburg-London-

München Collaboration, Phys. Rev. **138B**, 897 (1965).

<sup>10</sup>D. J. Schotanus *et al.*, Nucl. Phys. **B22**, 45 (1970).

<sup>11</sup>J. D. Jackson, Nuovo Cimento **34**, 1644 (1964).

<sup>12</sup>ABBBHLM Collaboration, Phys. Lett. **10**, 229 (1964); Nuovo Cimento **34**, 495 (1964).

<sup>13</sup>W. Michael and G. Gidal, Phys. Rev. Lett. **28**, 1475 (1972).

<sup>14</sup>K. Gottfried and J. D. Jackson, Nuovo Cimento **34**, 735 (1964).

<sup>15</sup>S. B. Treiman and C. N. Yang, Phys. Rev. Lett. **8**, 140 (1962).

<sup>16</sup>G. A. Ringland and R. L. Thews, Phys. Rev. **170**, 1569 (1968).

<sup>17</sup>K. Gottfried and J. D. Jackson, Nuovo Cimento **33**, 309 (1964).

<sup>18</sup>J. P. Ader *et al.*, Nuovo Cimento **56**, 952 (1968).

<sup>19</sup>G. Gidal *et al.*, Phys. Rev. Lett. **23**, 994 (1969).

<sup>20</sup>R. K. Yamamoto *et al.*, in *Proceedings of the XVI International Conference on High Energy Physics, Chicago-Batavia, Ill., 1972*, edited by J. D. Jackson and A. Rob-

- erts (NAL, Batavia, Ill., 1973), Vol. 1, p. 19.
- <sup>21</sup>M. Krammer and U. Maor, *Nuovo Cimento* 50A, 963 (1967).
- <sup>22</sup>M. Aderholz *et al.*, *Nuovo Cimento* 35, 659 (1965).
- <sup>23</sup>D. Brown *et al.*, *Phys. Rev. Lett.* 19, 664 (1967).
- <sup>24</sup>G. S. Abrams *et al.*, *Phys. Rev. Lett.* 25, 617 (1970).
- <sup>25</sup>Particle Data Group, LBL Report No. LBL-53, 1973 (unpublished).
- <sup>26</sup>M. Alston-Garnjost *et al.*, *Phys. Lett.* 36B, 152 (1971).
- <sup>27</sup>P. B. Johnson *et al.*, *Phys. Rev.* 176, 1651 (1968).
- <sup>28</sup>A. Kotański and K. Zalewski, *Nucl. Phys.* B22, 317 (1969).
- <sup>29</sup>G. Goldhaber *et al.*, *Phys. Lett.* 18, 76 (1965).
- <sup>30</sup>D. Brown *et al.*, *Phys. Rev. D* 1, 3053 (1970).
- <sup>31</sup>B. Haber *et al.*, *Nucl. Phys.* B17, 289 (1970).
- <sup>32</sup>A. Białas and K. Zalewski, *Nucl. Phys.* B6, 465 (1968).
- <sup>33</sup>A. Kotański and K. Zalewski, *Nucl. Phys.* B4, 559 (1968).
- <sup>34</sup>Bonn-Durham-Nijmegen-Paris-Strasbourg-Turin Collaboration, *Phys. Lett.* 28B, 72 (1968).